Transonic Free-to-Roll Analysis of Abrupt Wing Stall on Military Aircraft

D. Bruce Owens,* Francis J. Capone,† Robert M. Hall,‡ and Jay M. Brandon‡
NASA Langley Research Center, Hampton, Virginia 23681
and
Joseph R. Chambers§
Ball Aerospace Systems Division Fairborn, Ohio 45324-6269

Transonic free-to-roll and static wind-tunnel tests for four military aircraft—the AV-8B, the F/A-18C, the preproduction F/A-18E, and the F-16C—have been analyzed. These tests were conducted in the NASA Langley 16-Foot Transonic Tunnel as a part of the NASA/Navy/Air Force Abrupt Wing Stall Program. The objectives were to evaluate the utility of the free-to-roll test technique as a tool for predicting areas of significant uncommanded lateral motions and for gaining insight into the wing-drop and wing-rock behavior of military aircraft at transonic conditions. The analysis indicated that the free-to-roll results agreed well with flight data on all four models. A wide range of motions—limit-cycle wing rock, occasional and frequent damped wing drop/rock and wing-rock divergence—were observed. The analysis shows the effects that static and dynamic lateral stability can have on the wing-drop/rock behavior. In addition, a free-to-roll figure of merit was developed to assist in the interpretation of results and assessment of the severity of the motions.

Nomenclature

a	=	speed of sound
b	=	reference wing span
C_L	=	lift coefficient
C_l	=	rolling-moment coefficient
c_{ref}	=	reference wing chord (mean geometric chord)
f	=	frequency in cycles per second, Hz
g	=	acceleration of gravity
I_x	=	inertia about the roll axis
l	=	characteristic length
M	=	Mach number
n	=	geometric scale factor
p	=	roll rate
$p_{\mathrm{P-V}}$	=	free-to-roll figure of merit
$pb/2V_\infty$	=	reduced angular rate
q	=	pitch rate
q_∞	=	freestream dynamic pressure
Re	=	Reynolds number based on c_{ref}
r	=	yaw rate
S	=	reference surface area
t	=	time
V_∞	=	freestream velocity
V_∞^2/lg	=	Froude number
α	=	angle of attack
β	=	angle of sideslip
δ_{ht}	=	differential horizontal tail deflection
δ_{TEF}	=	trailing-edge flap deflection
θ	=	pitch angle
ρ_∞	=	freestream density
ϕ	=	roll angle
$\dot{\phi}$	=	roll rate, time derivative of the roll angle
$\ddot{\phi}$	=	roll acceleration, time derivative of the roll rate
ω	=	oscillatory frequency in radians per second, $=2\pi f$
$\omega b/2V_\infty$	=	Strouhal number

Subscripts

a	=	airplane
m	=	model

Introduction

MANY high-performance military aircraft have experienced abrupt, uncommanded lateral motion during transonic maneuvers.[1] One of the most recent aircraft experiences with such problems occurred for the preproduction F/A-18E/F when wing drop was encountered during the flight-test program. The problem was eventually mitigated by modifications to the wing automatic leading-edge flap schedule and by the addition of a porous fairing at the wing-fold location. Production versions of the aircraft incorporate these fixes and do not exhibit the problem. It was recognized that the fundamental understanding and engineering design methods for the mitigation of wing drop at transonic speeds was severely lacking. To obtain a better understanding of the cause of the uncommanded lateral motions of the F/A-18E/F during transonic wind-up turns and to offer design guidelines for future aircraft, the Abrupt Wing Stall (AWS) Program was developed. The details and results to date of this national program involving the NASA, Navy, Air Force, and universities are discussed in Refs. 1–18. This paper discusses the analysis of transonic free-to-roll (FTR) wind-tunnel tests that were conducted as a part of the AWS program.

The FTR test technique has been used by NASA at the Langley Research Center to assess the low-speed, high angle-of-attack characteristics of high-performance aircraft configurations for several decades. These tests have been used to successfully predict and analyze uncommanded rolling motions for generic and scaled models. With the exception of a semi-free-to-roll test conducted by Northrop and NASA Ames for the F-5A,[19] the use of the FTR test technique in the transonic regime has not been utilized to study uncommanded lateral motions. Reference 1 states that a loss in roll damping was the cause for many of the high-performance military aircraft to develop wing rock/drop. Inherently, the FTR test technique assesses the impact of roll damping. In general, the FTR test technique allows rolling motion to develop, which is a response to the unsteady,

nonlinear aerodynamics of the model. As pointed out in Ref. 1, the FTR test technique was not readily available for use in transonic stability and control tests.

As a part of the AWS Program, an exploratory transonic FTR test was conducted with a 9% preproduction F/A-18E model in the NASA Langley Transonic Dynamics Tunnel in the fall of 2000. This highly successful pathfinder test proved the utility of the FTR test technique in evaluating the uncommanded lateral motions of the preproduction F/A-18E. Based on the success of this pathfinder study, an operational test apparatus and technique was developed for the NASA Langley 16-Foot Transonic Tunnel (16-ft TT) to permit FTR studies for other military aircraft configurations. The tests were designed to evaluate the FTR test technique as a tool during normal transonic stability and control static force tests. Therefore, the FTR rig was designed with the objectives of using existing transonic wind-tunnel models and allowing rapid transition from the static test technique to the dynamic test technique with the same model in the same tunnel entry.[10]

The analysis of the FTR tests will be presented by first discussing the FTR test technique. Next, the scope and approach of the tests will be discussed. Finally, the results and discussion will be presented. The results and discussion section will present the interpretation of the rolling motions, the definition of the FTR figure of merit (FOM), and will conclude with individual discussions of the lateral motion (activity) for each aircraft. To obtain approval for releasing this paper to the public, quantitative information has been removed from most vertical scales as per guidelines from the U.S. Department of Defense.

Free-to-Roll Test Technique

The FTR test technique is a single-degree-of-freedom test method in which the model is free to roll about the longitudinal body axis. The overall objective of FTR testing is an early identification of potential uncommanded lateral motion problems (or lack thereof). If the results of static force-and-moment tests indicate that a potential exists for wing rock/drop, the FTR method can then be used to study the dynamic behavior. Inherently, the FTR technique evaluates unsteady, nonlinear aerodynamics. The technique allows for an estimation of the roll damping derivative C_{l_p}. In addition to estimates of aerodynamic parameters, if the model and test conditions are appropriately dynamically scaled estimates of full-scale motions (e.g., amplitudes, frequencies, and accelerations) could be made. Because the FTR tests are designed to be conducted with the same models, and even during the same test entry used for traditional static force-and-moment measurements, the models do not usually incorporate an active control system to stabilize the motions or duplicate the effects of the stabilization system of the full-scale aircraft.

Figure 1 shows kinematic relationships during the rolling motion. For a given pitch angle θ, as the model rolls from a wings-level condition the angle of attack α decreases, and angle of sideslip β increases in magnitude. The mathematical representations of the kinematics
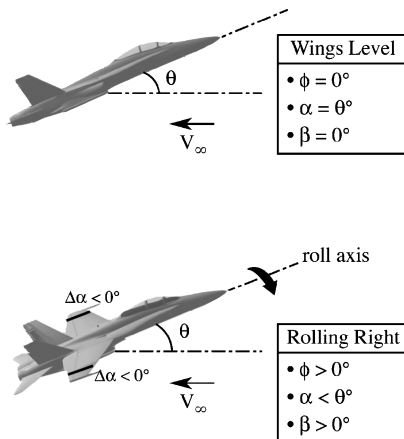

Fig. 1 Kinematic relationships during rolling motion at a fixed pitch and yaw angle.

are given as $\alpha = \tan^{-1}(\cos \phi \tan \theta)$ and $\beta = \sin^{-1}(\sin \phi \sin \theta)$. Also, note that for the FTR technique $p = \dot{\phi}$, $q = 0$, and $r = 0$. As shown in Fig. 1, the downgoing wing experiences an incremental increase in α. At the wing tips, this increment is equal to $\tan^{-1}(pb/2V_\infty)$. In a similar fashion, the up-going wing experiences a decrease in α of identical magnitude. If the model is in wing stall conditions, the rolling motion can result in undesirable dynamic behavior. Specifically, at a value of θ in the stall region the local sectional lift characteristics of the downgoing wing might experience a greater loss in lift than the up-going wing. This lift differential would then propel the motion, rather than damp the motion, and the model would exhibit a loss in roll damping. In other words, the value of C_{l_p} would become positive.

Governing Equation

The equation of motion for the FTR technique can be represented as $I_x \ddot{\phi}/qSb - C_{l_{\dot{\phi}}}(\dot{\phi}b/2V_\infty) - C_{l_\phi}\phi = C_{l_0}$. The governing equation was cast in terms of the Euler angle ϕ because this directly models the FTR motion about the longitudinal body axis. This differential equation can be nonlinear because the aerodynamic coefficients can be functions of θ, ϕ, $\dot{\phi}$, $\ddot{\phi}$, time, Mach number, etc. The foregoing equation is in the form of the classical mass-spring-damper system where C_{l_0} represents an aerodynamic forcing function for $\phi = 0$ deg; C_{l_ϕ} represents the spring constant, which, along with the inertia, determines the frequency of oscillation; and $C_{l_{\dot{\phi}}}$ represents the damping coefficient. Note that friction in the system can be accounted for in the damping term. In addition, the use of $C_{l_{\dot{\phi}}}$ and C_{l_p} is kinematically equivalent.

Because the governing equation for the FTR method contains the static derivative C_{l_ϕ} instead of C_{l_β}, it is advantageous to make ϕ sweep runs during the static force portion of the test. This allows for a clearer understanding of the static lateral stability that the model experiences while it rolls between some ϕ range. The C_l vs ϕ curve will define the steady-state value of C_{l_0}, the nonlinearity of the spring, the frequency of the motion, and nominal range of ϕ that the model will oscillate within. If hysteresis is present, then ϕ sweeps in both directions must be made in order to capture the full nonlinearity of the spring.

Dynamic Scaling

If the roll angle, roll rate, and roll accelerations that the wind-tunnel model experiences are to be scaled to flight, then certain specific dynamic similitude requirements must be met.[20] Obviously, for transonic testing Mach scaling must be used as in conventional static tests. However, additional similitude requirements exist for FTR testing. As Ref. 20 points out, in Mach scaling the ability to satisfy attitude scaling is dependent on satisfying Froude-number similitude. The following example from Ref. 20 demonstrates how the Froude number is related to attitude scaling. To match bank angle in flight during a coordinated turn having an instantaneous turn radius R and rate of turn $\Omega (= V_\infty/R)$, the bank angle is given by

$$\phi = \tan^{-1}(mR\Omega^2/W) = \tan^{-1}\left(V_\infty^2/Rg\right) = f\left(V_\infty^2/lg\right)$$

where m is the mass and W is the weight. A static test requires model attitude, control deflection, Mach number, and Reynolds-number similitude. In addition to these requirements, the FTR test also requires freestream velocity, dynamic pressure, inertia, reduced angular rate $pb/2V_\infty$, and Strouhal number $\omega b/2V_\infty$ (if the motion of the model is oscillatory) similitude. The ability to Froude scale and Mach scale simultaneously is practically impossible in wind-tunnel testing. Details of these similitude requirements are given in Ref. 20. An example of the impact of these requirements is given in Ref. 21. Dynamic scaling issues for the specific models tested will be addressed in a following section.

Roll-Damping-Derivative Estimation Method

Examination of the roll damping derivative C_{l_p} is instructive for understanding and mathematically representing the wing-rock motions. Estimations of C_{l_p} from the FTR tests can be made using

parameter identification (PID) methods. The method used in the current analysis utilized linear regression. The software used for computing C_{l_p} is a package of MATLAB® scripts developed at NASA Langley called SIDPAC.[22] The FTR motions are modeled in this approach using the governing equation just given assuming constant coefficients over a specified range of ϕ. Also, note that the actual parameter that is being computed is $C_{l_p} + C_{l_{\dot{\beta}}} \sin \alpha$.

Test Approach and Scope of Tests

Four airplane configurations were chosen to evaluate the FTR test technique and to compare wind-tunnel results with those obtained in flight. Two configurations (preproduction F/A-18E and AV-8B) are known to have wing-drop/rock characteristics over some of the flight envelope. Two others (F-16C and F/A-18C) do not exhibit such behavior in flight. This selection of flight vehicles allowed the FTR test technique to be used to discriminate between configurations with desirable and undesirable flight characteristics. Details of the models, test conditions, and FTR rig are given in Ref. 10. A short synopsis will be given here for convenience.

The models were tested on a FTR rig in the NASA Langley 16-ft TT. The geometric characteristics of the models are given in Table 1. The sketches of the models in Fig. 2 are to the same scale in order to convey the relative model sizes used in the test. Note that the preproduction F/A-18E model did not contain the porous wing-fold fairing. The flap configurations tested corresponded to those used in representative flight maneuvers. In the figures and discussion a flap set for the F/A-18C and preproduction F/A-18E is denoted as leading-edge (LE) flap/trailing-edge (TE) flap/aileron in degrees. The abbreviation for the F-16C is LE flap/TE flap in degrees. θ is used as the independent variable in the FTR tests because when the model rolls θ remains constant while α varies. The AV-8B model was tested at the following M and Re pairs: (0.3, 2.4×10^6); (0.5, 3.6×10^6); and (0.75, 4.5×10^6). The F/A-18C, F/A-18E, and F-16C models were tested at $0.8 \leq M \leq 0.9$. The nominal Reynolds number for these models was 3.6×10^6, 3.9×10^6, and 2.8×10^6, respectively.

A sketch of the FTR rig is shown in Fig. 3. As explained in Ref. 10, the FTR apparatus was designed and built for the 16-ft TT. When the apparatus is in a FTR mode, the rotary section of the FTR rig, the sting, the balance, and the model all rotate on two sets of bearings. The total roll inertia of all of these moving parts for each model is given the Table 1. This inertia is used to compute the aerodynamic rolling moment when the model is undergoing a rolling motion. To conduct static force tests, the model can be
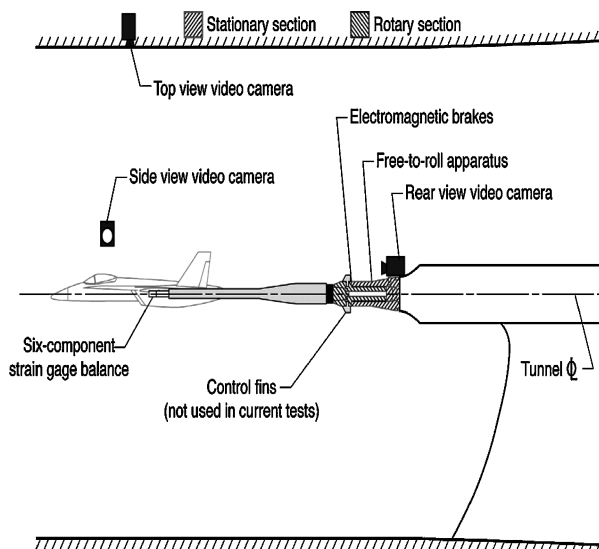
Table 1 Model geometric characteristics

Characteristic	AV-8B	F/A-18E	F/A-18C	F-16C
Scale, %	15	8	6	6.67
Mean aerodynamic chord, ft	1.246	1.048	0.917	0.755
Span, ft	4.55	3.34	2.25	2.07
Wing area, ft^2	5.18	3.2	1.44	1.33
Aspect ratio	4	3.5	3.5	3.2
Leading-edge sweep, deg	36	29.4	26.5	40
Length, ft	6.77	4.58	3.27	3.1
I_x, slug-ft^2	5.2	2.5	1.2	1.37

Fig. 2   Model sketches.

Fig. 3   Sketch of the NASA Langley 16-Foot Transonic Tunnel FTR apparatus.

held in a rigid position by a locking bar placed across the rotary and stationary parts. Switching between the static-force mode and the FTR mode required only 30 min. The rig has electric brakes that work much like automotive disc brakes. The brakes are used to arrest motion, as well as to set the model at specific initial roll angles. As shown Fig. 3, remotely controlled fins were placed on the rig to adjust model roll-angle trim. It was known that these fins would introduce error into the FTR technique, but it was hoped that the tares would either be quantifiable or only have a slight adverse effect. Unfortunately, during the rig checkout phase it was determined that the fins produced an unacceptable adverse effect, and they were removed from the apparatus for all of the tests. In addition, during the rig checkout phase an attempt was made to ascertain the amount of friction in the system.[10] The friction was found to be small relative to the expected values of roll damping; however, the effects of friction will be greater for smaller models. Ongoing friction analyses are attempting to quantify the effects of the FTR rig friction on aerodynamic coefficient estimates.

The procedure for conducting the FTR tests consisted of a static-force phase and a FTR phase. During the static-force phase, force-and-moment data were measured using a six-component strain-gauge balance. For some models, wing-root bending moment was also measured with strain gauges mounted in the wing. During the FTR tests, in addition to the aforementioned measurements the roll-angle time history was measured with a resolver having an accuracy of 0.067 deg. Also, video of the rolling motions from three different views was recorded.

For a given configuration, the static-force phase consisted mainly of α sweeps and was conducted first. Then, the locking bar was removed, and the FTR phase was conducted. During the FTR phase, three testing methods were utilized: continuous pitch sweeps, pitch pause, and ϕ offset. The continuous pitch sweeps were conducted by slowly pitching the model up through the desired θ range and then pitching the model back down through the θ range while the model is free to roll. This method is used to quickly find the θ range where wing rock exists, if at all, and permits for an assessment of any hysteresis effects in pitch angle. Various pitch rates were also used to assess pitch-rate effects on the development of the uncommanded lateral motions. Following the continuous pitch sweeps, pitch-pause points were taken. Pitch-pause points are taken to assess the lateral activity at specific pitch angles. In this procedure the model is held fixed with the wings level (± 2 deg) using the brakes. The model is then moved to the desired pitch angle. When on point, the brakes are released, and the ensuing motion is recorded. The precursor continuous pitch sweeps are used to determine over what range of α that finer increments in θ are needed. The pitch-pause points are used to
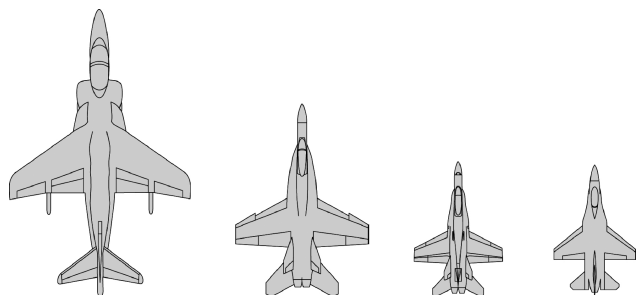
determine the tendencies of lateral motions to develop from a $\phi = 0$ and $\dot{\phi} = 0$ condition. Next, the ϕ-offset points are conducted by releasing the model from a $\phi \neq 0$ and $\dot{\phi} = 0$ condition, which induces a rolling motion by the action of the static lateral stability. This procedure will accomplish three objectives: 1) allow assessment of roll damping, 2) discover if the model will develop sustained lateral activity given an initial rolling motion if none existed before, and 3) determine if the induced rolling motion will impact the lateral activity seen before. After the FTR phase was completed, the locking bar was replaced for additional static force measurements. During this phase, ϕ sweeps and β sweeps were conducted in order to quantify the static lateral characteristics. The pitch angles for these sweeps were ones where significant lateral activity was seen during the FTR phase.

One caution regarding the application of the FTR test technique is the use of the method at low pitch angles. During FTR testing, the wings are leveled by the static lateral stability ($C_{l_\beta} < 0$). Recalling the kinematic relationships given earlier, if the model is disturbed from a wings-level condition at low pitch angles the model will roll to large bank angles in order to generate enough rolling moment caused by sideslip to counter this disturbance. Therefore, at low pitch angles the rolling motions can be difficult to interpret, especially if the model has out-of-trim roll characteristics or if the wind tunnel has significant flow angularity.

Results and Discussion

Interpretation of Results

During the FTR tests, a wide variety of rolling motions were observed. Based on a review of the static-force data, time-history traces of the roll angle, and estimations of C_{l_p}, the following discussion categorizes and gives an interpretation as to possible causes of these motions. As a first level of distinction between the rolling motions observed, an abrupt rolling motion that damps with only one or two small-amplitude overshoots will be termed wing drop (Fig. 4), and the more sinusoidal motions will be termed wing rock (Fig. 5). The motions will be categorized by number so that reference can be made to them in the specific discussions that follow.

Type 1—Limit-Cycle Wing Rock

This motion is characterized by wing rock for which the amplitude range is fixed and does not vary with time. Such motions can occur when C_{l_p} is near zero and C_{l_ϕ} is stable. Only approximate limit-cycle wing rock was observed (Fig. 5).

Type 2—Wing Rock with Constant Frequency but Varying Amplitude (Fig. 6)

This motion can occur because of the model rolling between regions of stable and unstable C_{l_ϕ} and C_{l_p}.
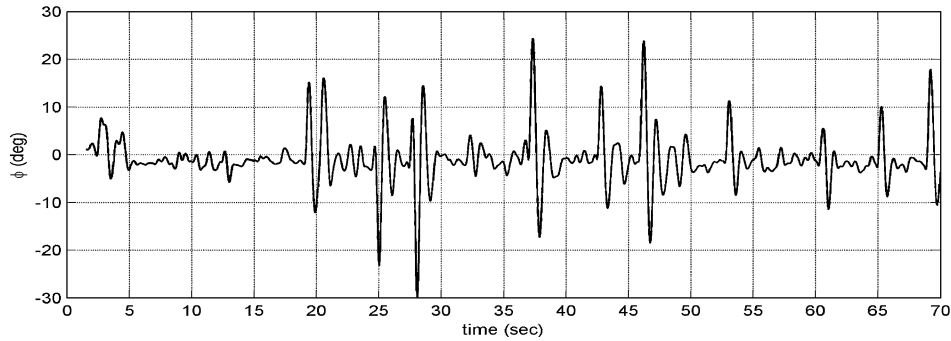

Fig. 4   Roll-angle time history showing wing drop for the F/A-18E: flap set 6/8/4, $M = 0.8$, and $\theta = 7.3$ deg.
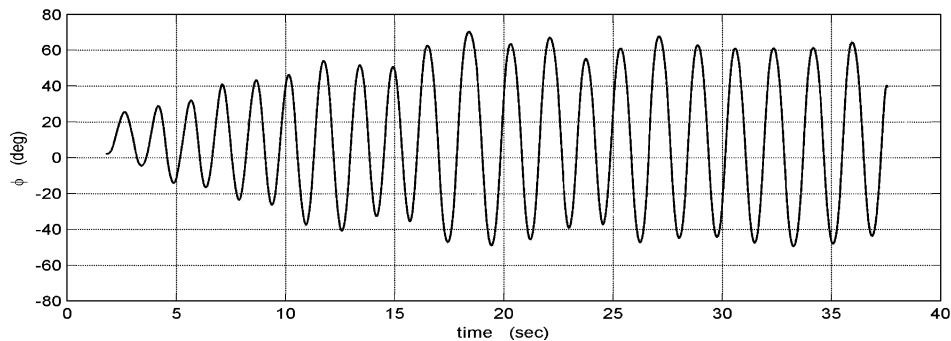

Fig. 5   Type 1 wing-rock motion of the AV-8B: 65% leading-edge root extension; $\delta_{\text{TEF}} = 25$ deg, $M = 0.3$, and $\theta = 18.5$ deg.
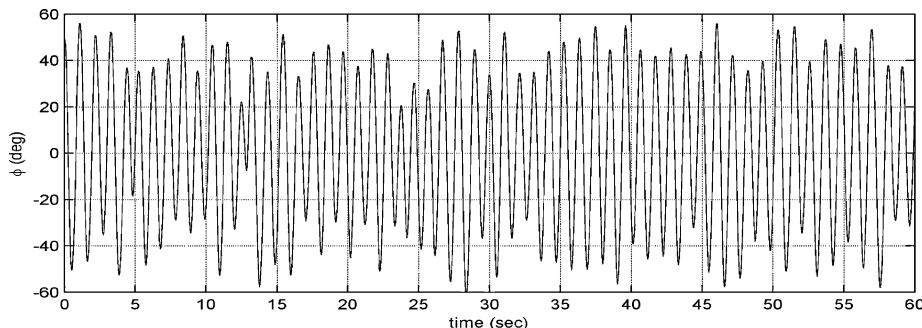

Fig. 6   Type 2 wing-rock motion of the preproduction F/A-18E: flap set 6/8/4, $M = 0.8$, and $\theta = 7.25$ deg.
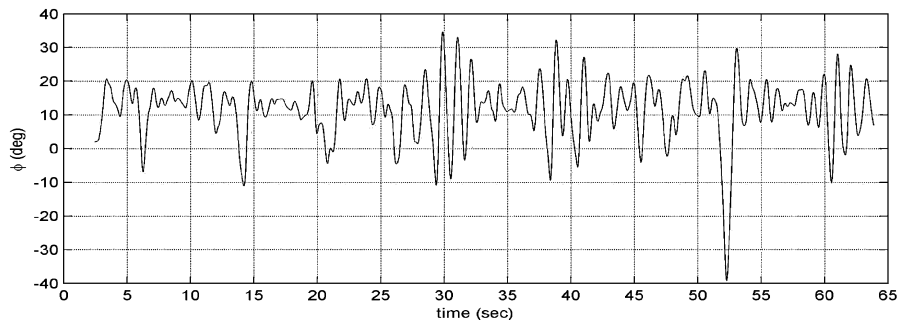
Fig. 7 Type 3 wing-rock/drop motion of the preproduction F/A-18E: flap set 15/10/5, $M = 0.8$, and $\theta = 8$ deg.
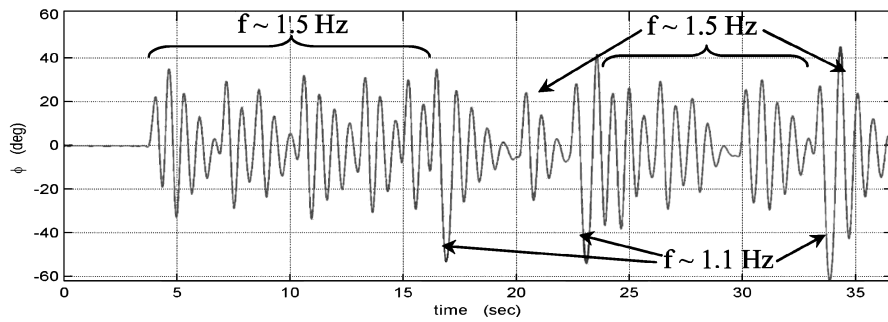

Fig. 8 Type 4 wing-rock events of the F/A-18C: flap set 10/12/0, $M = 0.85$, $\theta = 15$ deg, and $\delta_{ht} = -3$ deg.
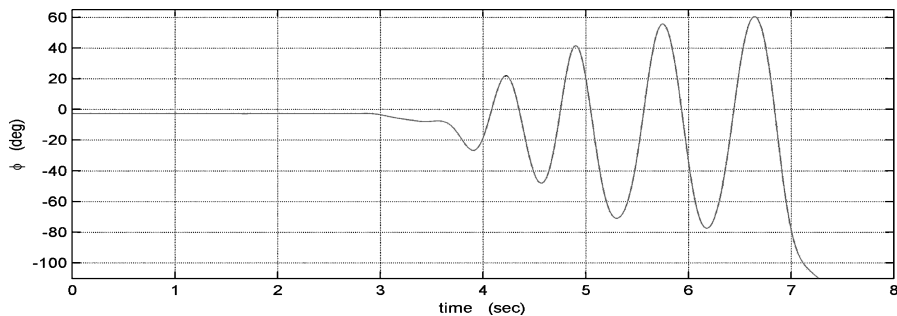

Fig. 9 Type 5 divergent rolling motion of the F/A-18C: flap set 10/12/0, $M = 0.85$, $\theta = 16.5$ deg, and $\delta_{ht} = -3$ deg.

Type 3—Occasional Damped Wing Drop and Wing Rock (Figs. 4 and 7)

Occasional means there can be many seconds between wing-drop/rock events where there is not any significant lateral activity. Type 3 tends to occur on the edge of stall and well after the stall. This motion is probably the result of unsteady variations in C_{l_0} with highly stable C_{l_ϕ} and C_{l_p}. Figure 7 shows the roll-angle time history of the preproduction F/A-18E model and is an example of type 3 rolling motions where both wing rock and wing drop occurred. At $t = 5$, 15, and 52 s the motions are wing drops. At $t = 30$, 40, and 60 s the motions are damped wing rock.

Type 4—Frequent Damped Wing Rock and Wing Drop (Fig. 8)

Type 4 tends to occur more often during the heart of the stall. This motion is probably caused for the same reason as type 3 except with a reduction in roll damping.

Type 5—Divergent Wing Rock (Fig. 9) and Wing Drop

The motion of type 5 is determined by the static and dynamic stability. If C_{l_ϕ} is unstable, then the model will roll over without oscillating. If C_{l_p} is unstable for all roll angles but has static stability, then the rolling motion will be a divergent roll oscillation as in Fig. 9.

What distinguishes types 1 and 2 from 3 and 4 is the response to the asymmetric wing stall. The sustained wing rock in types 1 and 2 appears to occur because the model experiences variations in C_{l_p}

and C_{l_ϕ} over the range of rolling motion. This statement is not meant to exclude the possibility of an additional superimposed aperiodic forcing function, for example, unsteady shock movements, which would contribute to the motion. However, in contrast to types 3 and 4 it is difficult to separate this superimposed forcing function from the regions of stable and unstable C_{l_p} and variations in C_{l_ϕ}. Types 3 and 4 behave more like an underdamped spring-mass-damper system with a forcing function that occurs when the roll rate is nearly zero. In other words, for types 3 and 4 C_{l_p} and C_{l_ϕ} are probably stable (and maybe even constant) over the range of rolling motion.

With the exception of having a perfect limit-cycle wing-rock motion, rolling motions of all five types were observed during the tests. All five types of motions can be initiated by abrupt (steady or unsteady) asymmetric wing stall. However, it was also seen that in some cases where abrupt asymmetric wing stall did not initiate the rolling motion the motion could be initiated by inducing a rolling motion. This result was accomplished by releasing the model from a nonzero roll angle. Detailed discussions for each of these motions will be given in the following sections.

FTR Figure of Merit

To discern the level of lateral activity, a FTR FOM was developed. This figure of merit needs to resolve significant activity from inconsequential activity. The first figure of merit used was a simple rating system based on amplitude of bank angle change. However,
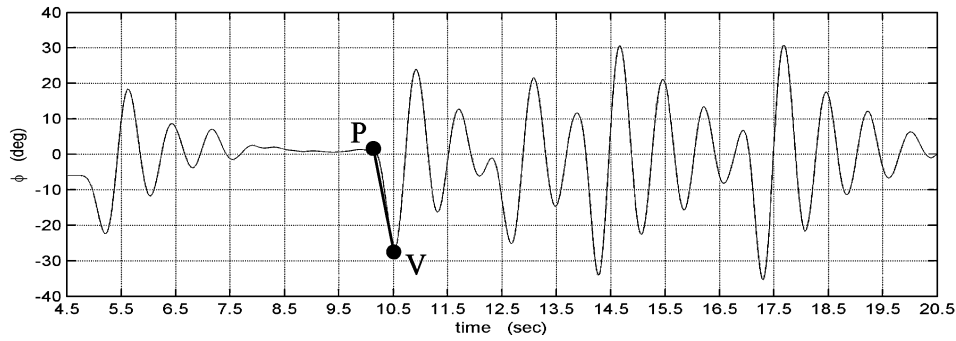
Fig. 10   Demonstrates how the FTR figure of merit is defined.

taking into account amplitude alone could be misleading because the rate of motion is ignored. That is, if a large amplitude occurs with a slow roll rate then it would be easily controlled. Taking into account just the magnitude of rates or accelerations alone could also be misleading because a large acceleration with a small amplitude change would not lead to a large deviation in the aircraft trajectory. Therefore, the figure of merit that was developed considered both amplitude and rate.

The FTR FOM was computed from a time history of the roll angle by the following procedure. First, the absolute value of the amplitude change from a maximum (peak) to its nearest minimum (valley) was determined. Then, this value is divided by the time it takes to roll through this amplitude change. This ratio is, of course, the slope of a line connected from the maximum to the minimum (Fig. 10). This quotient has the same dimensions as roll rate. Finally, this quotient is computed using all maximums and minimums. The FTR FOM p_{P-V} is the maximum of these ratios. Mathematically this can be stated as $p_{P-V} \equiv (|\Delta\phi/\Delta t|)_{\max}$. A FOM that uses the acceleration (i.e., the rolling moment) is also being investigated and can replace the present FOM.

The level of lateral activity for each of the models will mainly be shown using this FTR FOM. All FTR FOM shown are computed from pitch-pause FTR points. The range on the vertical scale of the FTR FOM plots is identical for plots of a given airplane. The same range was not used for all of the models because there was no expectation that the level of lateral activity should be the same for all airplanes given their different sizes and inertias. The FTR FOM plots present the amount of lateral activity as the dependent variable and the pitch angle as the independent variable. The parameters in the plot are the flap sets that correspond to those used in representative flight maneuvers (e.g., windup turn). Therefore, a relative measure of the lateral activity predicted by the FTR test technique that the aircraft would experience in flight is shown by plotting a symbol on the curve at the α where the aircraft flap schedule most closely matches the flap setting tested in the wind tunnel.

The FTR test technique is a single-degree-of-freedom method where the model is constrained to roll about the longitudinal body axis. In addition, it does not incorporate an active control system. Therefore, these considerations must be recognized when comparing the lateral activity observed on the FTR apparatus to those experienced by full-scale aircraft. In addition, similitude effects must be taken into account if the models are not dynamically scaled.

Effect of Dynamic Scaling

As mentioned in the Dynamic Scaling section, Froude and Mach scaling are both important in transonic FTR tests. Froude scaling ensures that the model attitudes are correct. In other words, the wing sectional angle of attack is correct. The reduced angular velocity, Strouhal number, and freestream scaling requirements depend heavily on the geometric scale factor. The 16-ft TT is an atmospheric tunnel so the ratio of tunnel-to-flight freestream velocity is on the order of 1.1 for a flight altitude of 25,000 ft. Unfortunately, the reduced angular velocity and Strouhal number are much lower than required to match flight. The effect is that the change in local wing

Table 2   Ratio of scaled-up test inertias to actual inertias

| | I_{x_m}/I_{x_a} | |
Model	Alt. = 15,000 ft	Alt. = 25,000 ft
AV-8B	4.7	3.4
F/A-18C	62	44
F/A-18E	20	15
F-16C	159	113

sectional angle of attack caused by roll rate will not be as large as it should. Therefore, if the wing-rock motions occur in a highly nonlinear flow region the model will not experience as large a deviation in wing flowfield structure as the full-scale aircraft. This, in turn, could impact the amount of roll damping.

Dynamic pressure must also be scaled properly. For Froude scaling, dynamic pressure is scaled by $(\rho_m/\rho_a)^n$. For Mach scaling, it is scaled by $(\rho_m/\rho_a)(a_m/a_a)^2$. Fortunately, at transonic Mach numbers in the 16-ft TT the density altitude is about 15,000 ft Therefore at a flight altitude of 15,000 ft dynamic pressure scaling is closely matched for Froude scaling and off by approximately 20% for Mach scaling.

Achieving inertia similitude is the same for Mach and Froude scaling and is given by

$$I_{x_m} = \frac{\rho_m}{\rho_a}\left(\frac{b_m}{b_a}\right)^5 I_{x_a}$$

Of course, because the model is only free to roll about the longitudinal axis then only the inertia scaling about this axis is required. This equation shows that the inertia is scaled by the fifth power of the geometric scale factor. To give an indication of how close this requirement was met, the model's roll inertia was scaled up to full-scale aircraft values at altitudes of 15,000 and 25,000 ft. Table 2 shows the ratio of the scaled inertia to the real airplane's inertia (for a nominal loading). The table shows that the AV-8B, the model with the greatest roll inertia, scaled more closely because of the larger span. The F-16C was furthest from proper inertia scaling. Although the F/A-18C and the F-16C are close in model inertia and span, the full-scale roll inertia for the F-16C is much less than the F/A-18C. The general effect of the higher inertia on the rolling motion is to act like a low-pass filter on the accelerations. For example, if the aerodynamic forcing function is broadband in nature[5] then the model's inertia might not allow it to react to the higher frequency content of the forcing function. The importance of the dynamic scaling is determined by the nonlinear dependence in the C_{l_0}, C_{l_ϕ}, and $C_{l_{\dot\phi}}$ terms on ϕ, $\dot\phi$, $\ddot\phi$, time, hysteresis, etc. If the aerodynamics vary nonlinearly, then a general assessment of the impact of improper dynamic scaling is not possible.

Hysteresis

It is not uncommon for aerodynamic hysteresis to be present especially in the stall region. Hysteresis was present in the static rolling moment vs ϕ data. The hysteresis in this static data was

measured using pitch-pause points where the model was sweep from $\phi = -90$ to 90 deg then back to $\phi = -90$ deg for a specified θ. In addition, hysteresis was observed during the FTR test phase when the model was continuously pitched up then back down. All of the FTR pitch-pause points were conducted with θ increasing. Detailed analysis of the hysteresis effect is not complete, but the possibility of its effect on the rolling motions should be considered.

Results for the Four Aircraft

AV-8B

The measured lateral activity of the AV-8B will be presented mainly using the FTR FOM. The FTR FOM for the AV-8B with the 65% leading-edge root extension (LERX) at $M = 0.3$ is shown in Fig. 11. The TE flap deflection is 25 deg, which the aircraft control system schedules for angles of attack above 15 deg. The rise in lateral activity occurs just after $\theta = 15$ deg, reaching a plateau around 16 deg. Type 1 wing-rock motions occurred in the range of θ from 16 to 19 deg. Figure 5 shows an example of the wing-rock motion observed in this θ range. The figure shows that rolling motions increase in amplitude, finally reaching an approximate limit-cycle oscillation. The wing rock has a frequency of 0.6 Hz with approximately $\phi = \pm 50$-deg amplitude about a $\phi = 10$-deg offset. In flight, lateral activity was observed in approximately the same α range at Mach numbers close to 0.25. The model exhibited wing-rock divergence (type 5) in the range 19.5 deg $< \theta < 20.5$ deg.

Figure 12 shows the lateral activity for the AV-8B at $M = 0.5$ with the 65% LERX and $\delta_{TEF} = 25$ deg. This flap setting is on schedule for the α range above 15 deg. The plot shows the onset of lateral activity at $\theta = 14.5$ deg but peaks with a larger magnitude between $\theta = 16.5$ and 17.5 deg. This is in good agreement with the α range observed in flight, which occurred between $\alpha = 15$ and 18 deg. For the $\theta = 14.5$ to 16 deg range, the lateral activity were of the type 4 motions. In the $\theta = 16.0$ to 17.5 deg range, the events were of the type 1 and 2 wing rock. The roll damping derivative C_{l_p} was estimated using the PID method in the $\theta = 16.0$ to 17.5 deg range and found to be neutrally stable. This is in agreement with C_{l_p} estimates reported in Ref. 23, which were computed using flight data at $M = 0.6$.

The FTR FOM plot in Fig. 13 shows that at $M = 0.75$ for the AV-8B with the 65% LERX, $\delta_{TEF} = 10$ deg configuration that again the θ range of lateral activity on the FTR rig and flight has good agreement. Note that the actual TE flap schedule for the α range above 8.5 deg is about 12.5 deg. The lateral activity observed in the

Fig. 13 Lateral activity of the AV-8B at $M = 0.75$ with the 65% LERX and $\delta_{TEF} = 10$ deg.
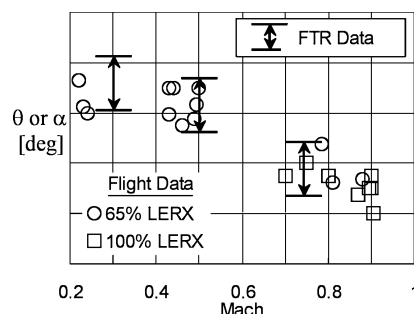
Fig. 14 Summary plot for the AV-8B comparing the θ range of FTR activity to the α range of flight activity.

FTR tests in the $\theta = 10.5$ to 11.5 deg range was the type 4 wing rock. The wing rock in the $\theta = 12$ to 14 deg range was the type 2 motion.

By comparing the three FTR FOM plots, it is observed that the FOM rating increases significantly with Mach number. This rise in the rating is caused by the dynamic pressure increase from $M = 0.3$ to 0.75. This result points out the need for the FTR FOM to account for q_∞. As mentioned in the FTR Figure of Merit section, the present FTR FOM is still under development.

Figure 14 shows a summary comparison of the FTR lateral activity compared to flight lateral activity. The FTR FOM was not presented for the 100% LERX configuration, but the results as compared to flight are also shown in this figure. The comparison is only of the θ range and Mach range of unacceptable lateral activity, not the type of lateral activity. The θ range of wing-rock events that were captured by the FTR test technique show good agreement with flight data at all three Mach numbers—0.3, 0.5, and 0.75.

F/A-18C

The F/A-18C model did not experience any significant lateral activity on flap schedule but did exhibit wing-rock/drop events far off flap schedule. The following summarizes the lateral activity observed using the FTR FOM. Two detailed analyses are given. During the FTR phase of the test, the horizontal tails were deflected differentially to trim out an inherent rolling moment offset. During the initial static-force phase, the tails were not deflected. After the FTR phase static-force runs were made with the tails deflected. The static data with the tails in both positions are utilized in the following discussions.

Figure 15 shows the FTR FOM plot for the F/A-18C at $M = 0.80$ for the four flap sets tested. In agreement with flight, no significant lateral activity occurred on flap schedule. There is a rise in activity where the aircraft is on schedule at $\theta = 12$ deg, but this is considered very mild. The data show significant lateral activity off flap schedule. The lateral activity observed for the 0/0/0 flap configuration at $\theta = 11.5$ and 12 deg was of the type 2 wing rock motion. The 6/8/0 flap configuration showed type 2 wing rock motion for the $\theta = 11.5$ to 13.5 deg range. At $\theta = 14.5$ and 15 deg the model actually diverged in roll. The lack of lateral activity at $\theta = 14$ deg when there is such severe activity within a degree underscores the sensitivity to θ. The 10/12/0 flap configuration exhibited type 2 wing rock in the $\theta = 14$ deg area but actually diverged at $\theta = 15$ and 15.5 deg. In general, the 15/12/0 set did not show any significant lateral activity
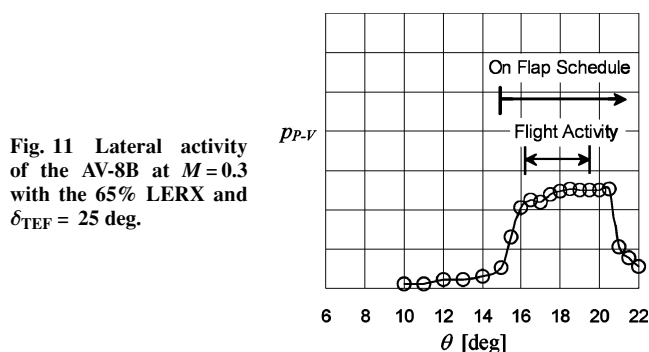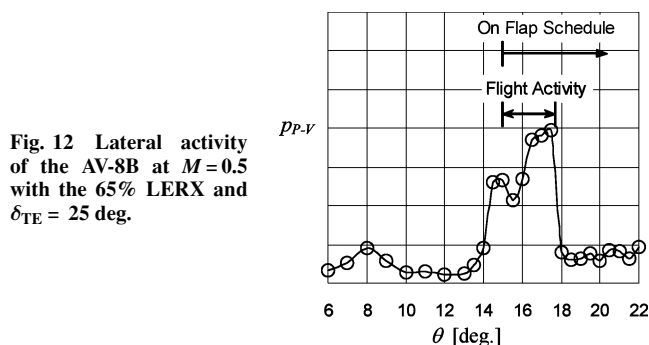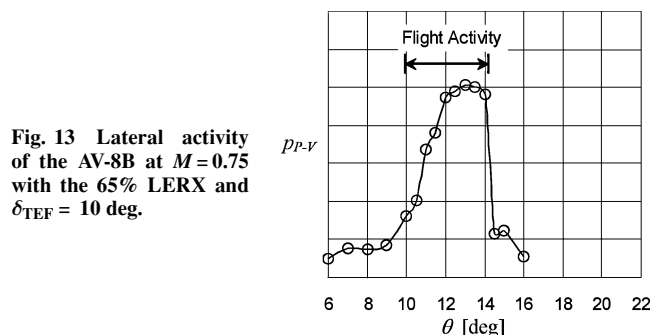

Fig. 11 Lateral activity of the AV-8B at $M = 0.3$ with the 65% LERX and $\delta_{TEF} = 25$ deg.

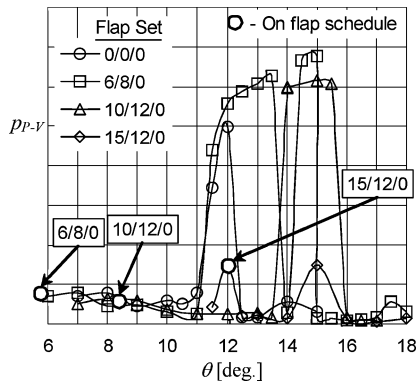**Fig. 12 Lateral activity of the AV-8B at $M = 0.5$ with the 65% LERX and $\delta_{TE} = 25$ deg.**

Fig. 15 Lateral activity of the F/A-18C at M = 0.80.

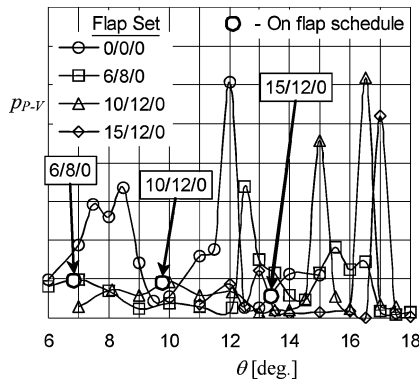
Fig. 16 Lateral activity of the F/A-18C at M = 0.85.
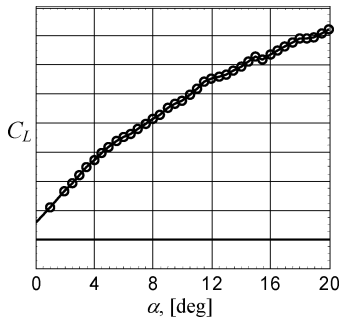

Fig. 17 Lift characteristics for the F/A-18C: flap set 10/12/0, $M = 0.85$, $\beta = 0$ deg, and $\delta_{ht} = -3$ deg.
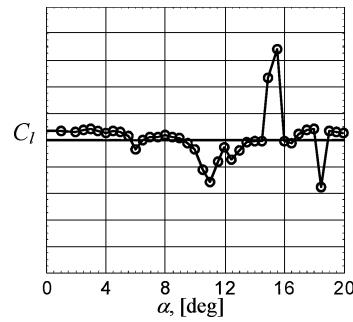

Fig. 18 Static rolling moment for the F/A-18C: flap set 10/12/0, $M = 0.85$, $\beta = 0$ deg, and $\delta_{ht} = -3$ deg.
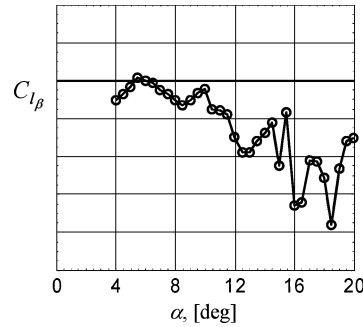

Fig. 19 Static lateral stability near zero roll angle for the F/A-18C: flap set 10/12/0, $M = 0.85$, and $\delta_{ht} = 0$ deg.
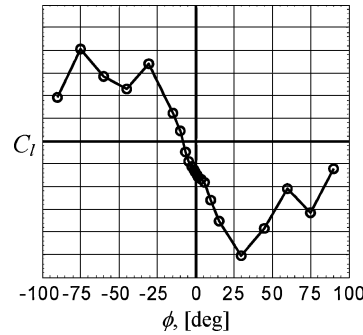

Fig. 20 Static rolling moment for the F/A-18C: flap set 10/12/0, $M = 0.85$, $\theta = 15$ deg, and $\delta_{ht} = 0$ deg.

over the θ range. The rolling motion that was observed at $\theta = 12$ and 15 deg could be classified as low activity type 3 wing rock.

Figure 16 shows the FTR FOM results for $M = 0.85$ with the four flap configurations tested. In agreement with flight, the F/A-18C model did not experience lateral activity on flap schedule. As at $M = 0.80$, there was lateral activity when significantly off flap schedule. The 0/0/0 flap configuration showed type 2 wing-rock events in the $\theta = 7.5$ to 8.5 deg range. At $\theta = 12$ deg, the model experienced type 2 wing-rock events with mild type 3 just prior to this θ. The 6/8/0 flap set only experienced significant type 4 wing-rock activity at $\theta = 12.5$ deg. There was only very mild type 3 wing rock at $\theta = 13$ deg. The 10/12/0 flap configuration exhibited type 4 wing rock at $\theta = 15$ deg. At $\theta = 16.5$ deg the θ model experienced roll divergence (type 5). A detailed analysis of the two points at $\theta = 15$ and 16.5 deg will follow. The only significant activity for the 15/12/0 flap configuration was a divergent wing rock (type 5) at $\theta = 17$ deg. There was very mild type 3 wing rock at $\theta = 13$ deg.

The wing-rock behavior for the 10/12/0 flap configuration at $M = 0.85$ and $\theta = 15$ deg is shown as a time-history plot of the roll angle in Fig. 8. The model is released from a wings-level condition at approximately 4 s. Immediately the model experiences a wing-rock event probably caused by the asymmetric stall of the wings. The ensuing lateral activity is the frequent damped wing rock (type 4). The static lift, rolling moment, and lateral stability curves as a function of α are shown in Figs. 17–19, respectively. The static

lateral stability curve was computed using α sweeps at $\beta = \pm 2$ deg and with no differential deflection in the horizontal tails. Looking at the $\alpha = 15$ deg point on these curves, the wing-rock event occurred where there is a negative break in the lift curve, a positive spike in the rolling moment curve, and rapid increase in static lateral stability. These are all classical indications that lateral activity could occur in the α region. Lamar and Hall[9] give detailed analysis of static FOMs for predicting lateral activity for all four aircraft. In addition, Capone et al.[10] compares the static FOMs against the FTR FOM. Estimations of C_{l_p} by the PID method show that it is nearly constant with a value of -0.3 over the $\phi = \pm 30$ deg range.

The model reacts to the abrupt asymmetric wing stall by a damped wing-rock motion of near constant frequency ($\sim$1.5 Hz). The wing rock damps out in about three to four oscillations. As the motion comes to a stop, the wings abruptly and asymmetrically stall again, and the motion repeats itself. The first oscillation of most of the wing-rock events occurs over a ±30-deg amplitude range. When the model stays within this amplitude range, the oscillation frequency is nearly constant at 1.5 Hz. However, when the abrupt asymmetric wing stall is severe enough to cause the oscillation to exceed this amplitude there is a significant change in frequency of this oscillation ($\sim$1.1 Hz).

Insight into the understanding for this frequency change and the ±30-deg amplitude range can be gained by observing the static rolling moment values over this range of ϕ. Figure 20 shows the static rolling moment as a function of ϕ for $\theta = 15$ deg and the horizontal tails undeflected. As a side note, the C_{l_0} in this curve is of the opposite direction than in Fig. 18. A number of repeat α sweeps ($\beta = 0$ deg) were made for this configuration. Around $\alpha = 15$ deg the rolling moment spiked both with positive and negative values

of almost equal magnitude. This indicates the unsteadiness in the flowfield and points out the importance of repeat runs to the complete understanding of the wing rock motions. Figure 20 shows a relatively linear C_{l_ϕ} slope in the $\phi = \pm 30$ deg range. Beyond $\phi = \pm 30$ deg, C_{l_ϕ} is reduced. Recall that C_{l_ϕ} acts as a spring constant and, therefore, affects the frequency. When the abrupt asymmetric wing stall causes the model to roll into the nonlinear spring range, then the resulting motion will change frequencies. As can be seen in the roll angle time-history plot, the frequency decreases when the model oscillates past $\phi = \pm 30$ deg. Note that the model rolling motion will be an integrated effect of having a nonlinear spring force. An example in the preproduction F/A-18E section will show the resulting motion when C_{l_ϕ} and C_{l_p} are both varying over the ϕ range.

The other insight to be gained from this example is that the amplitude of the rolling motions mainly stayed in the ϕ range of where the local slope of $C_{l_\phi} \leq 0$. This was generally true for all of the models tested when they exhibited type 1–4 wing-rock/drop motions. This result has been observed before in low-speed high-angle-of-attack research (for example, see Ref. 24). Therefore, a rough rule of thumb is that the shape of the C_l vs ϕ curve can be used to predict the steady-state frequency and approximate maximum range of wing-rock amplitude for type 1–4 motions.

Figure 9 shows an example of wing-rock divergence (type 5). The roll-angle time history for the 10/12/0 flap configuration at approximately $\theta = 16.5$ deg is shown in this figure. The estimated value of C_{l_p} is +0.3. Figure 19 shows that the model has stable static lateral stability near $\phi = 0$ deg. The motion is started as a result of an initial asymmetry with the growth in amplitude caused by the propelling value of C_{l_p}. Furthermore, Fig. 21 shows the static rolling moment vs ϕ data for $\theta = 16$ deg and the horizontal tails undeflected. Although this curve is not for the exact same θ under discussion, the general nature of this curve is probably representative at $\theta = 16.5$ deg. The frequency changes from 1.5 Hz for the first oscillation to 1.1 Hz for the final oscillation. This frequency change is caused by the nonlinearity in C_{l_ϕ} across the ϕ range. An unstable trim point probably exists in the range of the $\phi = 95$ to 115 deg. Therefore, once the model's bank angle exceeds the amplitude at this unstable trim point it drove itself into the soft limit set by the brakes.

Figure 22 shows the FTR FOM plot for $M = 0.90$. As with $M = 0.80$ and 0.85, no significant lateral activity was experienced by the model on flap schedule, which is in agreement with flight.

Fig. 21 Static rolling moment as a function of roll angle for the F/A-18C: flap set 10/12/0, $M = 0.85$, $\theta = 16$ deg, and $\delta_{ht} = 0$ deg.
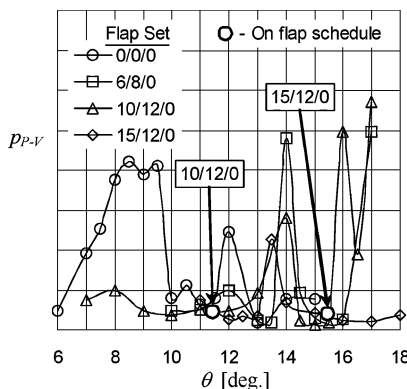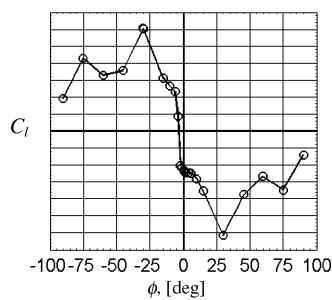

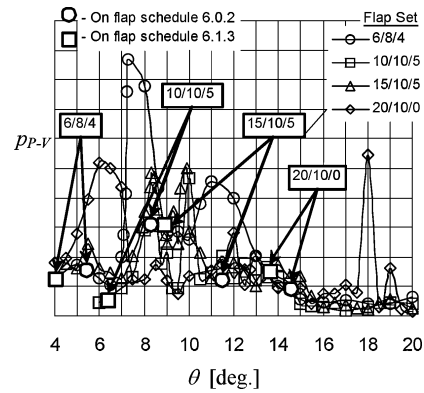Fig. 22 Lateral activity of the F/A-18C at $M = 0.90$.

Fig. 23 Lateral activity of the preproduction F/A-18E at $M = 0.80$.

There was however significant wing-rock/drop off flap schedule. The 0/0/0 flap configuration showed significant type 2 lateral activity in the $\theta = 8$ to 9.5 deg range. The milder activity at $\theta = 12$ deg was type 3 wing-rock motions. The 6/8/0 flap configuration experienced severe type 2 wing-rock motions at $\theta = 14$ deg and type 3 wing rock at $\theta = 17$ deg . The 10/12/0 flap set showed type 3 wing rock at $\theta = 14$ deg and experienced severe type 2 wing rock at $\theta = 16$ deg. The 15/12/0 only experienced a mild type 3 wing rock at $\theta = 13.5$ deg.

Preproduction F/A-18E

The preproduction F/A-18E model was tested on the FTR rig at $M = 0.8$ and 0.9 with four different flap configurations. In the discussion reference is made to the v6.0.2 flap schedule and the v6.1.3 flap schedule. The v6.0.2 flap schedule was in place during the flight-test program when the wing-drop problem was discovered. The v6.1.3 flap schedule was the flap set that gave an 80% solution to the wing-drop problem. The FTR results showed significant lateral activity for both flap schedules.

The lateral activity experienced by the preproduction F/A-18E model at $M = 0.80$ for four different flap configurations is shown by the FTR FOM plot in Fig. 23. The plot shows that there was significant lateral activity on the v6.0.2 flap schedule at $\theta = 8$ deg (10/10/5 flap set) and on the v6.1.3 flap schedule at $\theta = 9$ deg (15/10/5 flap set). There were also significant wing-rock/drop events off schedule as well. The 6/8/4 flap configuration exhibited type 3 wing drop around $\theta = 7$ deg and again around $\theta = 11$ deg. The model exhibited severe type 2 wing rock in between $\theta = 7.25$ and 8 deg range. A detailed look at the $\theta = 7.25$ deg point will be shown subsequently. In the range of $\theta = 8$ to 12 deg, the rolling motions were of type 3 and type 4. The 10/10/5 and 15/10/5 configurations exhibited type 3 and type 4 wing rock and wing drop when they became active. The lateral activity experienced by the 20/10/0 configuration was mainly type 2 wing rock in the $\theta = 5.5$ to 7 deg range while the activity observed at $\theta = 18$ deg was type 3 wing drop.

The model undergoing severe type 2 wing rock is shown by a roll-angle time history plot in Fig. 6 for the 6/8/4 configuration at $M = 0.8$, $\theta = 7.25$ deg. The time history is characterized by a rolling motion with amplitude and frequency varying between ± 10 deg at 1.1 Hz to ± 50 deg at 0.95 Hz. Most of the energy in the signal is at the 0.95-Hz frequency. Data of the static rolling moment C_l and dynamic damping derivative C_{l_p} vs ϕ, given in Figs. 24 and 25 respectively, are employed to understand this motion. The C_l vs ϕ curve shows that the spring constant C_{l_ϕ} is nearly constant in the $\phi = \pm 35$ deg range. Beyond $\phi = 35$ deg, C_{l_ϕ} is reduced. As pointed out in the first F/A-18C example, when the oscillations exceed the range of $C_{l_\phi} < 0$ the frequency changes because of the integrated value of the nonlinear spring constant. Also, as observed in the F/A-18C example, the maximum range of amplitude is roughly determined by range of $C_{l_\phi} \leq 0$. In contrast to the F/A-18C example, the motion does not fully damp to near-zero roll rate. This can be explained by the C_{l_p} vs ϕ curve in Fig. 25. This curve shows that the roll damping varies significantly with ϕ. C_{l_p} is propelling between
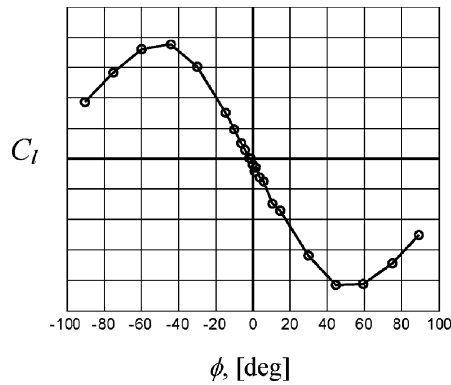
Fig. 24   Static rolling moment for the preproduction F/A-18E: flap set 6/8/4, $M = 0.8$, and $\theta = 7.2$ deg.
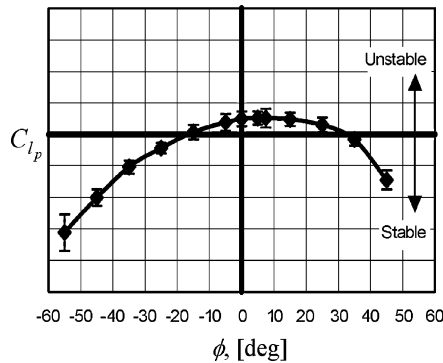

Fig. 25   Variation of the roll damping derivative with roll angle for the F/A-18E: flap set 6/8/4, $M = 0.8$, and $\theta = 7.25$ deg. 3-σ error bars are shown.
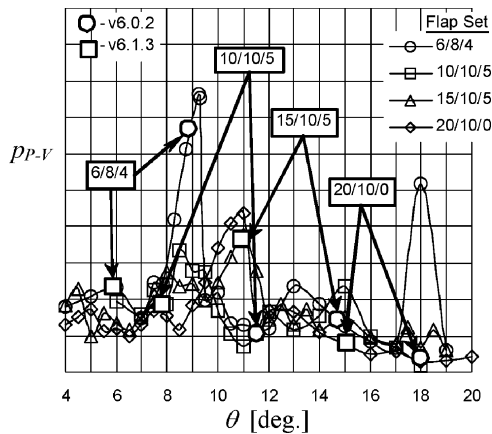

Fig. 26   Lateral activity for the preproduction F/A-18E at $M = 0.90$.

-15 deg $< \phi < 30$ deg . Outside of this ϕ range the model exhibits a significant increase in damping. This character has been observed before in the low-speed research (for example, see Ref. 25). This C_{l_p} character is in contrast to the F/A-18C example, where C_{l_p} was always damping and nearly constant with ϕ.

Figure 26 shows the FTR FOM plot for $M = 0.9$. The plot shows that there is significant lateral activity on the v6.0.2 flap schedule at $\theta = 8.5$ deg (6/8/4 flap set) and on the v6.1.3 flap schedule at $\theta = 11$ deg (15/10/5 flap set). The lateral activity for all four flap configurations consisted only of the type 3 and type 4 wing-drop events. In other words, at $M = 0.9$ the model never showed a tendency to develop limit-cycle wing rock, which is in contrast to $M = 0.8$. It is known (see Ref. 9) that C_{l_β} is weaker at $M = 0.9$ than at $M = 0.8$ and might explain this behavior.

A summary of the θ and Mach range of FTR activity compared to flight data is shown in Fig. 27 for Mach numbers of 0.8 and 0.9. The data shown are where the airplane and the model had approximately
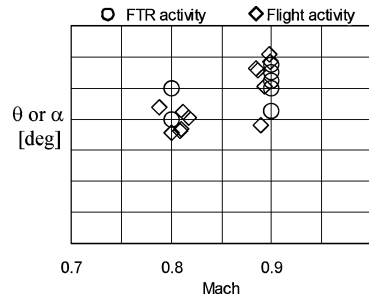

Fig. 27   Summary plot for the preproduction F/A-18E comparing the θ range of FTR activity to the α range of flight activity for $M = 0.8$ and 0.9.
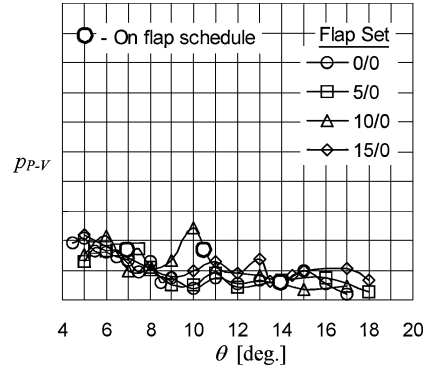

Fig. 28   Lateral activity of the F-16C for $M = 0.8$.
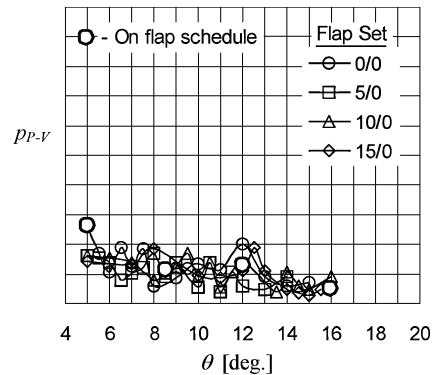

Fig. 29   Lateral activity of the F-16C for $M = 0.9$.

the same flap deflection and Mach number at the time of a lateral activity event. As with the AV-8B flight comparison, the correlation is only of the θ and Mach range of unacceptable lateral activity, not the type of lateral activity. This figure shows good agreement between the FTR results and the flight data.

F-16C

The level of lateral activity at $M = 0.80$ for the F-16C model is depicted in Fig. 28 using the FTR FOM. In agreement with flight, there is no significant lateral activity. What is unique about the F-16C compared to the other airplanes is that it exhibited no significant lateral events across the entire θ range. There is more lateral activity at the lower pitch angles, but this is primarily caused by the model responding to disturbances in the tunnel under the influence of a weak spring constant C_{l_ϕ}. Figure 29 shows the FTR FOM plot for $M = 0.90$. The amount of lateral activity is slightly different from that at $M = 0.80$, but overall there is no significant lateral activity or changes in lateral activity over the θ range. The behavior of the F-16C model at both Mach numbers is in agreement with flight.

Observations

The following is a list of observations from the FTR tests:
1) A better understanding of the wing-rock/drop motions was achieved by having static C_l vs ϕ data.

2) Static repeat runs were required to capture unsteady variations in the static rolling moment curve.

3) Pitch-sweeps, pitch-pause, and ϕ-offset type FTR runs were necessary to assess the conditions for which the model would develop lateral activity.

4) During the pitch-pause points, sometimes it was required to stay on condition for more than 30 s before the model experienced an uncommanded lateral motion.

5) The ability to start each pitch-pause point at zero roll angle and zero roll rate provided a rigorous assessment of potential lateral activity.

Summary

Transonic free-to-roll (FTR) and static wind-tunnel tests for four military aircraft—the AV-8B, the F/A-18C, the preproduction F/A-18E, and the F-16C—have been analyzed. These tests were conducted in the NASA Langley 16-Foot Transonic Tunnel as a part of the NASA/Navy/Air Force Abrupt Wing Stall Program. The objectives were to demonstrate the utility of the free-to-roll test technique as a tool for identifying areas of significant uncommanded lateral activity during ground testing and for gaining insight into the wing-drop and wing-rock behavior of military aircraft at transonic conditions. The analysis can be summarized as follows:

1) A figure of merit (FOM) was developed to assist in discerning the severity of lateral motions. Using this FOM, it was shown that the FTR test technique identified conditions where lateral activity occurred for the AV-8B and preproduction F/A-18E in an α range that correlates with flight. The FOM predicted no significant lateral activity for the F/A-18C and F-16C on flap schedule, which is in agreement with flight. This figure of merit is still under investigation, and other FOMs can be developed.

2) The lateral activity observed during the tests was categorized into five different types. Analyses of some of these types were given and showed the relationship between the lateral activity behavior, the static data, the static lateral stability derivative C_{l_ϕ}, and dynamic damping derivative C_{l_p}.

3) It was observed that the C_l vs ϕ curve indicated the nonlinearity of the spring constant, the frequency of the wing-rock motion, and the approximate ϕ range of damped or limit-cycle wing rock/drop.

4) Hysteresis was present in the static C_l vs ϕ curve and in the free-to-roll continuous pitch sweeps. The effect of hysteresis is still under analysis.

5) Dynamic scaling issues are of concern and are being investigated. Even so, with the FTR results showing good agreement with flight it can be concluded that the models do not have to be dynamically scaled to make predictions of wing-rock/drop susceptibility.

Acknowledgments

References

[1]Chambers, J., and Hall, R., "Historical Review of Uncommanded Lateral-Directional Motions at Transonic Conditions," *Journal of Aircraft*, Vol. 41, No. 3, 2004, pp. 436–447; also AIAA Paper 2003-0590, Jan. 2003.

[2]Hall, R., and Woodson, S., "Introduction to the Abrupt Wing Stall (AWS) Program," *Journal of Aircraft*, Vol. 41, No. 3, 2004, pp. 425–435; also AIAA Paper 2003-0589, Jan. 2003.

[3]McMillin, N., Hall, R., and Lamar, J., "Understanding Abrupt Wing Stall with Experimental Methods," AIAA Paper 2003-0591, Jan. 2003.

[4]Woodson, S., Green, B., Chung, J., Grove, D., Parikh, P., and Forsythe, J., "Understanding Abrupt Wing Stall (AWS) with CFD," AIAA Paper 2003-0592, Jan. 2003.

[5]Schuster, D., and Byrd, J., "Transonic Unsteady Aerodynamics of the F/A-18E at Conditions Promoting Abrupt Wing Stall," *Journal of Aircraft*, Vol. 41, No. 3, 2004, pp. 485–492; also AIAA Paper 2003-0593, Jan. 2003.

[6]Forsythe, J., and Woodson, S., "Unsteady CFD Calculations of Abrupt Wing Stall Using Detached-Eddy Simulation," AIAA Paper 2003-0594, Jan. 2003.

[7]Parikh, P., and Chung, J., "A Computational Study of the AWS Characteristics for Various Fighter Jets: Part I, F/A-18E & F-16C," AIAA Paper 2003-0746, Jan. 2003.

[8]Chung, J., and Parikh, P., "A Computational Study of the Abrupt Wing Stall (AWS) Characteristics for Various Fighter Jets: Part II, AV-8B and F/A-18C," AIAA Paper 2003-0747, Jan. 2003.

[9]Lamar, J., and Hall, R., "AWS Figure of Merit (FOM) Developed Parameters from Static, Transonic Model Tests," AIAA Paper 2003-0745, Jan. 2003.

[10]Capone, F., Owens, B., and Hall, R., "Development of a Free-to-Roll Transonic Test Capability," *Journal of Aircraft*, Vol. 41, No. 3, 2004, pp. 456–463; also AIAA Paper 2003-0749, Jan. 2003.

[11]Owens, B., Capone, F., Hall, R., Brandon, J., Cunningham, K., and Chambers, J., "Free-to-Roll Analysis of Abrupt Wing Stall on Military Aircraft at Transonic Speeds," *Journal of Aircraft*, Vol. 41, No. 3, 2004, pp. 474–484; also AIAA Paper 2003-0750, Jan. 2003.

[12]Roesch, M., and Randall, B., "Flight Test Assessment of Lateral Activity," AIAA Paper 2003-0748, Jan. 2003.

[13]Green, B., and Ott, J., "F/A-18C to E Wing Morphing Study for the Abrupt Wing Stall Program," AIAA Paper 2003-0925, Jan. 2003.

[14]Kokolios, A., and Cook, S., "Use of Piloted Simulation for Evaluation of Abrupt Wing Stall Characteristics," AIAA Paper 2003-0924, Jan. 2003.

[15]Capone, F., Hall, R., Owens, B., Lamar, J., and McMillin, N., "Recommended Experimental Procedures for Evaluation of Abrupt Wing Stall Characteristics," *Journal of Aircraft*, Vol. 41, No. 3, 2004, pp. 448–455; also AIAA Paper 2003-0922, Jan. 2003.

[16]Woodson, S., Green, B., Chung, J., Grove, D., Parikh, P., and Forsythe, J., "Recommendations for CFD Procedures for Predicting Abrupt Wing Stall (AWS)," AIAA Paper 2003-0923, Jan. 2003.

[17]Cook, S., Chambers, J., Kokolios, A., Niewoehner, R., Owens, B., Page, A., and Roesch, M., "An Integrated Approach to Assessment of Abrupt Wing Stall for Advanced Aircraft," AIAA Paper 2003-0926, Jan. 2003.

[18]Hall, R., Woodson, S., and Chambers, J., "Accomplishments of the AWS Program and Future Requirements," AIAA Paper 2003-0927, Jan. 2003.

[19]Hwang, C., and Pi, W., "Some Observations on the Mechanism of Aircraft Wing Rock," AIAA Paper 78-1456, Aug. 1978.

[20]Wolowicz, C. H., Bowman, J. S., and Gilbert, W. P., "Similitude Requirements and Scaling Relationships as Applied to Model Testing," NASA TP 1435, Aug. 1979.

[21]Brandon, J., and Foster, J., "Recent Dynamic Measurements and Considerations for Aerodynamic Modeling of Fighter Airplane Configurations," AIAA Paper 98-4447, Aug. 1998.

[22]Morelli, E., "System Identification Programs for Aircraft (SIDPAC)," AIAA Paper 2002-4704, Aug. 2002.

[23]Stevenson, S., Holl, D., and Roman, A., "Parameter Identification of AV-8B Wingborne Aerodynamics for Flight Simulator Model Updates," AIAA Paper 92-4506-CP, Aug. 1992.

[24]Brandon, J. M., and Nguyen, L. T., "Experimental Study of Effects of Forebody Geometry on High Angle-of-Attack Stability," *Journal of Aircraft*, Vol. 25, No. 7, 1988, pp. 591–597.

[25]Nguyen, L., Yip, L., and Chambers, J., "Self-Induced Wing Rock of Slender Delta Wings," AIAA Paper 81-1883, Aug. 1981.